COBEM 2021 26th International Congress of Mechanical Engineering
November 22-26, 2021, Virtual Congress, Brazil

COB-2021-1511
NUMERICAL SIMULATION OF HYDRAULIC CONVEYING OF SOLID PARTICLES THROUGH A NARROW ELBOW

Elmar Anton Schnorr Filho
elmar.aschnorr@gmail.com
Nicolao Cerqueira Lima
nicolaol@hotmail.com
Erick de Moraes Franklin
franklin@fem.unicamp.br
School of Mechanical Engineering, University of Campinas - UNICAMP, Rua Mendeleyev, 200, Campinas, SP, Brazil

Abstract. *Elbows are ubiquitous elements in industrial pipelines and are subjected to erosion when a solid phase is present in the flow. This work presents a numerical investigation of a solid-liquid flow through a very-narrow elbow pipe, i.e., when the ratio between pipe and particle diameters is small. In the very-narrow case, some particular phenomena like the formation of plugs and even jamming may develop. Here, we investigate the dynamics of particles with 6 mm diameter and density of 1140 kg/m3 generated randomly at a horizontal inlet of a 25.4 mm-ID elbow pipe. The particles are subjected to a fluid flow with inlet mean velocities ranging from 0.06 m/s to 0.1 m/s. The horizontal section has a length of 5D, the vertical section has a length of 2.5D and the elbow radius is 1D. To simulate the transport of solid particles in the very-narrow case we make use of a resolved approach of the CFDEM software, which is a free open-source software that combines LIGGGHTS, for the discrete element method (DEM), and the well-known OpenFOAM, for the continuous phase. The resolved method simulations were first validated against experimental results and showed good agreement for the fluid dynamics. Then, we investigated the effect of different combinations of fluid velocity and particle inlet rate. We observed that the flow pattern varies with the fluid velocity, where, for low velocities, we have an almost static bed in the lower part of the horizontal section that extends until the elbow. We also found the particle rate saturation associated to each flow velocity, i.e. the maximum number of particles that enter the domain for a given fluid velocity. To the authors' knowledge this is the first time a study with very-narrow pipes considering elbows using a resolved method is presented. This work intends to enlighten the particle dynamics in this particular situation.*

Keywords: *resolved method, CFD-DEM, very-narrow pipe, elbow*

1. Introduction

Particulate materials are very relevant in human life, for they appear in different forms, like powders, grains and sands, covering more than 10% of Earth's surface. A few examples of granular materials are: coal, gravel, agricultural products (e.g. rice, soy, beans), chemical and pharmaceutical products like inks and pigments. Such materials are so bountiful that their processing corresponds to almost 10% of all energy spent in the world, standing just behind the water in a scale of importance in human life (Duran, 2012). Likewise, the combination of solids and fluids is also very present in nature, for example, in river beds, in the defrosting of a glacier or in the formation of dunes in deserts. Not only they appear together in nature but also in industry. The relevance of both materials leads, naturally, to the development of processing techniques. For decades hydraulic conveying of solid particles has been used in mining, chemical and food industries. It consists on using a fluid, usually water, flowing along a pipeline and taking advantage of drag forces to drive particles to a desired location (Uzi and Levy, 2018). It is a viable and efficient alternative to trucks and rails for transporting continuously high amounts of commodities, like coal, bitumen, ores and grains. It also could be employed in processing plants to quickly transport these raw materials between different locations. However, these raw products appear in a broad range of sizes, shapes and physical properties, and pipelines may have complex geometries with elbows and tees, making the design of hydraulic conveying systems more complex. Therefore, due to high amount of control variables and parameters, the prediction of flow pattern, pressure drop or friction loss inside these pipes becomes a challenge (Vaezi *et al.*, 2018; Zhou *et al.*, 2019).

The combination of bend pipes with flows involving a solid fraction is a subject that has been receiving much of attention due to the undesirable, yet unavoidable, phenomena that can arise like erosion, for example, which, if not controlled, can evolve to leaks, failures and potential injuries. Besides, the attrition between particles can lead to a degradation of the product quality as well (Uzi and Levy, 2018; Parsi *et al.*, 2014; Li *et al.*, 2019). Elbows and tees are ubiquitous elements in pipelines and its abruptly change of flow direction makes them more susceptible to erosion due

to particle impact. Numerous erosion estimation models based on experiments were developed in order to predict when and where there are more degradation of the pipe (Chen *et al.*, 2004). Bourgoyne Jr *et al.* (1989) conducted experiments about diverter systems and studied how sand particles in gas and liquid flows affect different geometries of elbows, tees and elbows with a vortice zone. They also proposed an erosion rate equation. Shirazi *et al.* (1995) developed a semi-empirical model to account for wear in tees and elbows with varied diameters. They merged experimental results in a simple geometry with numerical simulations performed by a 2D-CFD code with a Lagrangian tracking of particles in a time-averaged fluid field.

In addition to the phenomena arising from different pipe geometries, it is worth to notice that the ratio between particle and pipe diameter has also a great influence on the flow dynamics due to the high confinement of particles. Cúñez and Franklin (2020) investigated jamming and crystallization in very-narrow fluidized beds and found that, after decelerating the flow velocity to values closer than the minimum fluidization velocity, grains become crystallized and form an organized structure. They also found that the grain type is a predominant characteristic in the defluidization and moderately fluidization conditions.

The above-mentioned studies are just a few of which, over the years, have been developed to describe and predict solid-liquid or solid-gas flow characteristics. Due to the complex nature of the problem, predicting the flow behavior by changing parameters such as flow velocity, tube and particle diameter, or other physical properties is not an easy task. For that reason, the use of numerical simulations to evaluate the effects of such parameters became a good alternative.

Some conveniences of numerical simulations over experiments are the practicality of changing flow parameters, *e.g.* physical properties or geometries, the ability of making flow measurements that are not feasible or sometimes impossible of performing experimentally, and also the possibility of investigating critical conditions without any risks. Zhang *et al.* (2012) investigated, using a CFD-DEM coupling scheme, the erosion of slurry flow with solid particles in a 90° degree elbow pipe by changing the flow velocity and the elbow orientation. They found that the fluid velocity has an influence on the particle impact force on the wall, while the elbow orientation influences the puncture point location. The ratio between the pipe and the particle diameters was in the range of 6 to 50. Peng and Cao (2016) studied the erosion caused by a gas-solid flow in a 90° elbow pipe using a two-way coupling Eulerian-Lagrangian approach. The particles diameter varied between $100\ \mu m$ and $350\ \mu m$, while the pipe diameter ranged from $41\ mm$ to $304\ mm$. They investigated the influence of several parameters such as elbow radius, pipe diameter, fluid inlet velocity and bend orientation. Based on the particles trajectories, they found that the profile of the particle concentration is intricate with the erosion profile.

Despite of the amount of works in this area, the reliability of numerical simulations stands upon a good model to describe the system in study. The Euler-Lagrange approach can basically be separated in two distinct groups: the unresolved approach and the resolved one. The former is founded on using a locally averaged Navier-Stokes equations for the fluid and the correlations to describe the fluid-particle interactions, like drag and lift forces. The latter makes the coupling between fluid and solid by actually computing the flow around each particle. Not only this approach does not rely on specific correlations, but also makes possible the usage of a CFD-DEM method when particles are larger than the computational mesh. Such scenarios are present when particles are relatively large in comparison to the pipe dimension, or when the flow requires a small-refined CFD mesh (Mondal *et al.*, 2016). As a drawback, the resolved method demands a larger cell refinement over the particles and as a consequence has a greater computational cost. Cúñez and Franklin (2019) investigated experimentally and numerically, using an unresolved method, a solid-liquid fluidized bed in a very-narrow tube. The numerical simulations capture the dynamics and length scales of plugs observed in experiments, and provided the information of the contact network between the particles, confirming their influence on the plug formation. Mondal *et al.* (2016) compared both the resolved and unresolved approaches on bridge formations with large particles on a solid-liquid flow. They observed that the unresolved approach does not provide good results at high particle concentrations because the grid size becomes comparable to the inter-particle separation distance and this leads to an incorrect estimate of the hydrodynamic interaction between particles.

According to previous works, elbows are a widely used element in industrial pipes: it interacts with the flow and affects the particle motion. In addition, the level of particle confinement in narrow and very-narrow tubes can generate other motion patterns. Therefore, the main objective of this work is to investigate the hydraulic transport of solid particles through a very-narrow elbow pipe by changing some flow parameters. We make use of a resolved approach from the CFDEM software, which is a free open-source software that combines both the well-diffused OpenFOAM software, used for the continuous phase, and LIGGGHTS, used for the discrete phase. The numerical model was first validated against experimental results found in literature. To the authors' knowledge this is the first time that a study combines particles in a very-narrow tube with an elbow using a resolved method. This work intends to shed a light in the dynamics of this particular case of solid-fluid flow.

2. Model Description

Particle-fluid flow models are divided in two major groups: treating particles as a continuum media (Euler-Euler) or as a discrete element (Euler-Lagrange) (Zhou *et al.*, 2010). One well-established numerical Euler-Lagrange model is the coupled CFD-DEM approach (Zhou *et al.*, 2019; Zhu *et al.*, 2007, 2008), which combines Discrete Element Method

(DEM), first proposed by Cundall and Strack (1979), with Computational Fluid Dynamics (CFD). In this work we make use of the open-source CFDEM software (www.cfdem.com), which couples the well-known OpenFOAM CFD software, responsible for handling the Eulerian phase, together with the DEM software LIGGGHTS (Hager *et al.*, 2012), used to calculate the particle-particle interaction.

2.1 Solid Phase

The Discrete Element Method (DEM) proposed by Cundall and Strack (1979) treats each particle in a Lagrangian framework. The particles are considered to be perfect spheres and can perform two types of motion, translation and rotation. Thus, their motion are given by Newton's second law. For a particle i with radius r_i, the equations of motion are given by (Kloss *et al.*, 2012):

$$m_i \frac{d\mathbf{u_i}}{dt} = \mathbf{F}_{f,i} + \mathbf{F}_{b,i} + \sum_{j \neq i}^{Np} (\mathbf{F}_{c,ij}) + \sum_{k \neq i}^{Nw} (\mathbf{F}_{c,ik}) \tag{1}$$

$$I_i \frac{d\omega_\mathbf{i}}{dt} = \sum_{j \neq i}^{Np} (\mathbf{T}_{c,ij}) + \sum_{k \neq i}^{Nw} (\mathbf{T}_{c,ik}) \tag{2}$$

where $\mathbf{u}_i$ is the particle linear velocity and ω_i is the angular velocity. m_i is the mass and I_i is the moment of inertia. $\mathbf{F}_{c,ij}$ and $\mathbf{F}_{c,ik}$ are, respectively, the contact force between particle *i* and particle *j* and the contact force between particle *i* and wall *k*. $\mathbf{T}_{c,ij}$ and $\mathbf{T}_{c,ik}$ are the torque in the particle-particle and particle-wall contact, respectively. $\mathbf{F}_{f,i}$ is the force that fluid exerts on the particle. $\mathbf{F}_{b,i}$ is the body force, considered here only by the gravity contribution. In DEM, the contact between particles is usually represented by an overlap between two bodies. So, the contact forces presented in equation 1 can be decomposed into a normal and a tangential component. Here, we apply the soft sphere approach, that models the contact force as a spring-dashpot system. The spring accounts for the deformation of the particle and the dashpot accounts for the energy dissipation. Normal and tangential contact forces between particles i and j can be decomposed as (Kloss *et al.*, 2012):

$$\mathbf{F}_{cn,ij} = \left(-k_n \delta_{n,ij}^{3/2} - \eta_n \mathbf{u}_{ij} \cdot \mathbf{n}_{ij}\right) \mathbf{n}_{ij} \tag{3}$$

$$\mathbf{F}_{ct,ij} = \left(-k_t \delta_{t,ij} - \eta_t \mathbf{u}_{s,ij} \cdot \mathbf{t}_{ij}\right) \mathbf{t}_{ij} \tag{4}$$

where n and t are subscripts representing the normal and tangential direction. k and η are the spring and dashpot coefficients. δ represents the overlap between the particles. $\mathbf{n}_{ij}$ is the vector that links particles centers. $\mathbf{u}_{ij}$ is the relative velocity and $\mathbf{u}_{s,ij}$ is the slip velocity at the contact point. $\mathbf{t}_{ij}$ is the tangential vector, defined as $\mathbf{u}_{s,ij}/|\mathbf{u}_{s,ij}|$. The above relations also hold for a particle-wall collision. The contact forces in this work are modeled following the Hertz-Mindlin and Deresiewicz model (Di Renzo and Di Maio, 2004).

2.2 Fluid Phase

The fluid motion is computed in an Eulerian frame. The equations that govern its motion are the incompressible Navier-Stokes equations with appropriate boundary and initial conditions. The algorithm used by OpenFOAM is based on the Finite Volume Method (FVM). In this work, we make use of a resolved approach, where the fluid flow is computed around each particle and their interactions come directly by solving the Navier-Stokes equations. This method is suitable in cases where the particle size overcomes the cell size (Mondal *et al.*, 2016). The resolved approach used is based on the immersed boundary method presented by Peskin (1972). In this method, only one pressure and velocity field for both phases exists and the regions covered by the particle assume its velocity, but describes a rigid body motion. Following Shirgaonkar *et al.* (2009), the governing equations are:

$$\frac{\partial \mathbf{u}_f}{\partial t} + \mathbf{u}_f \cdot \nabla \mathbf{u}_f = -\frac{\nabla P}{\rho_f} + \nu_f \nabla^2 \mathbf{u_f} \qquad \text{in } \Omega_f \tag{5}$$

$$\nabla \cdot \mathbf{u}_f = 0 \qquad \text{in } \Omega_f \tag{6}$$

With initial conditions:

$$\mathbf{u}_f(\mathbf{x}, t = 0) = \mathbf{u}_0(\mathbf{x}) \qquad \text{in } \Omega_f \tag{7}$$

Boundary conditions:

$$\mathbf{u}_f = \mathbf{u}_\Gamma \qquad \text{on } \Gamma \tag{8}$$

And solid-fluid interface conditions:

$$\mathbf{u}_f = \mathbf{u}_s \qquad \text{on } \Gamma_s \tag{9}$$

$$\boldsymbol{\sigma} \cdot \mathbf{n} = \mathbf{t} \qquad \text{on } \Gamma_s \tag{10}$$

where, Ω_f and Ω_s are the domain represented by the fluid and the solid phases, respectively. Γ is the CFD boundary and Γ_s the interface between the solid and the fluid. $\mathbf{u}_f$ is the fluid velocity, $\mathbf{u}_s$ is the solid velocity, $\mathbf{u}_\Gamma$ is the velocity boundary condition for the fluid, $\mathbf{u}_0$ is the initial condition for the fluid velocity, σ is the stress tensor, $\mathbf{n}$ is a vector pointing outwards the solid surface and $\mathbf{t}$ is the traction vector of the fluid acting on the solid surface.

The equations 9 and 10 are responsible for the coupling between both phases. The former matches the velocity between phases (no-slip condition at the solid boundary) and the latter is responsible for the tension that the fluid exerts on the particle, *i.e.* the drag force. The force acting on each particle is obtained by integrating the boundary condition in Eq. 10 over the body's boundary Γ_s, where the velocity used for the force calculation is weighted by the void fraction distribution on the interface. The same weighting average can be applied to the buoyancy force on each particle, when it is considered. Finally, the force exerted by the fluid on each particle is given by:

$$\mathbf{F}_d = \sum_{c \in V_{\Omega_S}} \left(-\nabla P + \mu_f \nabla^2 \mathbf{u}_f\right)(c) \cdot V(c) \tag{11}$$

where V_{Ω_S} represents all cells covered or partially-covered by the solid and $V(c)$ is the cell volume.

2.3 Numerical method

The fluid motion and its interaction with the solid phase are implemented in CFDEM according to the following algorithm (Kloss *et al.*, 2012):

(i) The DEM outputs the particles positions, velocities, radius in the domain at a certain time-step.

(ii) A void fraction model identifies the region covered by the particles and its interface, generating a smooth transition between phases.

(iii) The force that the fluid exerts on the particle is calculated using the velocity and the pressure fields, according to Eq. 11.

(iv) The fluid flow is calculated using the PISO (pressure-implicit with splitting of operators) loop, neglecting the presence of the particles.

(v) The particles velocities are incorporated in the fluid velocity field, which is later corrected to satisfy mass conservation.

(vi) The pressure is once more corrected and the routine restarts from step (i).

The numerical method presented in this section was used in all numerical simulations of this work. If any other configuration was used, it will be explicitly described. In this work, a dynamic grid refinement was used in order to improve the mesh refinement around the particles. In addition to resolve the flow more accurately, it also reduces the computational cost by refining only the locations where particles are presented. The dynamic meshing tool was set with level 2, which means that the cells, where the particles are located, are divided by half two times in each direction. The PISO algorithm was used to solve fluid flow equations, where we used 2 pressure corrections and 2 non-orthogonal correctors. The non-orthogonal correctors are necessary due to the use of the dynamic grid refinement utility, which creates some tetrahedral elements. For the temporal discretization we used the Euler discretization scheme, which is a first-order, bounded, implicit scheme.

3. Model Validation

The validation of the numerical model was carried out by reproducing experimental results found in literature. Here, we present the validation of the drag coefficient on a sphere with the experimental results from Brown and Lawler (2003). Other model validations looking for different aspects of the solid-particle interaction were conducted but, for the sake of brevity, they were omitted.

3.1 Drag Coefficient on a sphere

To validate the immersed boundary algorithm used in this work we made use of experimental results of drag coefficient on a sphere from Brown and Lawler (2003). The drag force of a fluid acting on a sphere was acquired for different Reynolds number and the comparison with the experimental results was made through the following correlation for the drag coefficient:

$$C_d = \frac{8F_d}{\pi d_p^2 \rho_f u_f^2} \tag{12}$$

where F_d is the drag force, d_p is the particle diameter, ρ_f is the fluid density and u_f is the free stream velocity. The simulations were conducted in a rectangular domain of 60 mm square base and 90 mm height. A particle of $d_p = 6$ mm is fixed in a position 30 mm from the inlet, and subjected to a horizontal uniform flow, as shown in Fig. 1a.

The fluid properties were set to $\rho_f = 1000$ kg/m^3 and $\mu_f = 0.001$ $Pa.s$ and its velocity was varied to cover a Reynolds number range, based on particle diameter, between 1 and 1000. We used a fixed value for the fluid velocity at the inlet and a zero-gradient condition for the outlet. The walls have a no-slip condition. For the pressure, the boundary conditions were zero-gradient at the inlet and fixed value at the outlet. The simulations were conducted using three distinct initial mesh refinement, namely 2, 4 and 6 CFD cells per particle diameter. The CFD time-step was chosen to satisfy the condition of Courant number less than one and therefore varied between 5×10^{-3} s to 5×10^{-4} s for a Reynolds number range of 1 to 1000, respectively. A coupling factor of 10 was used, hence the DEM time-steps varied between 5×10^{-4} s to 5×10^{-5} s.

The simulations were conducted until the velocity and pressure residues stabilized. The results for the 6 cells/d_p refinement are presented in Fig. 1b. The numerical simulation results for an initial mesh configuration of 6 cells per particle diameter presented a good agreement with the experimental ones, specially for the Reynolds number ranging from 5 to 700.

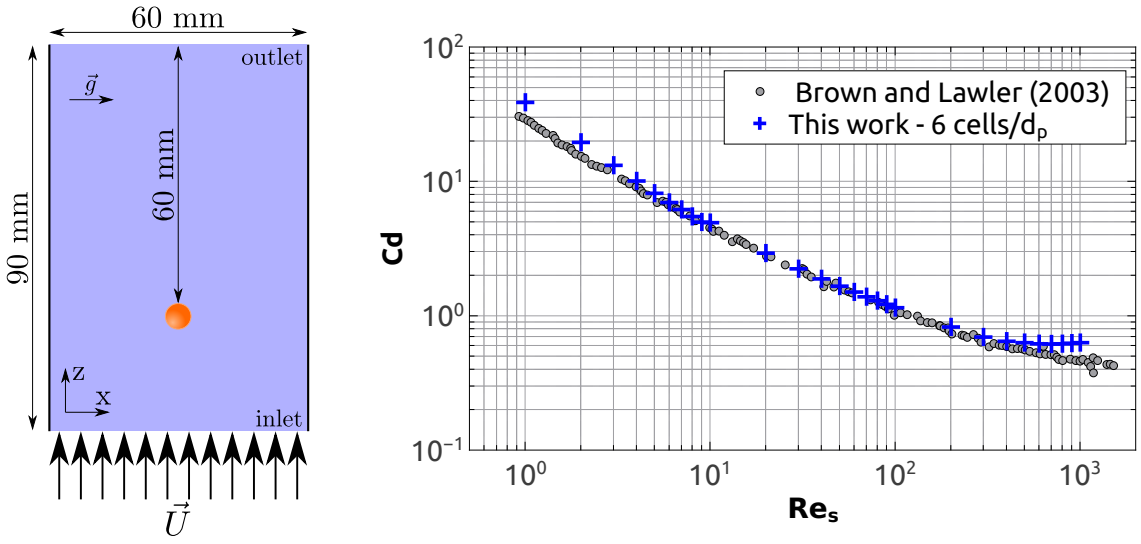

(a) (b)

Figure 1: (a) Drag coefficient; and (b) geometry of the drag coefficient simulation.

4. Numerical Setup

The main simulations were conducted in a pipe with an elbow of 25.4 mm-ID initially filled with water. The pipe has a horizontal section of length 2.5D and a vertical section of length 5D. The elbow radius of curvature is equal to pipe internal diameter. The inlet is localized at the horizontal section and the outlet at the vertical section. The CFD domain is presented in Fig. 2. The initial mesh refinement is 6 cells per particle diameter in the pipe section but in the flow direction the mesh is coarser. We observed that this approach reduces the computational cost and still provides satisfactory results. The mesh consists of 38016 hexahedral elements. The OpenFOAM dynamic meshing utility with a refinement level of 2 was used, which, during the simulation leads to, approximately, 2.5 million CFD cells. Initially, there are no particles inside the domain. Then, particles with 6 mm diameter and density of 1140 kg/m^3 are randomly generated at the inlet (blue section of Fig. 2), in a specific particle rate and subjected to a flow ranging from 0.06 m/s to 0.1 m/s.

Fluid enters the domain at a fixed value, exits with a zero-gradient condition and has a no-slip condition at the wall. The pressure at the inlet has a zero-gradient condition and at the outlet a fixed value one. The time-step used for the CFD

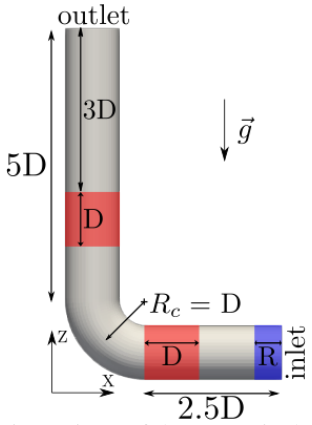

Figure 2: Dimensions of the numerical simulation.

was 1×10^{-3} s and for the DEM was 2×10^{-5} s, leading to a coupling factor of 50, which is in the recommended range in order to obtain accurate solutions (Mondal *et al.*, 2016). The CFD and DEM time-steps were also in accordance to the Courant number criterion and the collision time-span based on Hertz theory. It is worth to notice that the particle Young's modulus used in the simulations is two orders of magnitude lower than the real Young's modulus. This allow us to enhance DEM time-step and still capture the particle dynamics (Mondal *et al.*, 2016). The time-span of the simulations presented in Sec. 5. was 8 s. Particles properties were chosen to represent Nylon 6,6 and are listed in Tab. 1.

Table 1: Parameters used in simulation.

Particle diameter d (mm)	6
Particle density ρ_s (kg/m^3)	1140
Young's Modulus E (MPa)	33
Poisson's ratio ν	0.41
Restitution coefficient e	0.5
Coefficient of friction μ	0.25
Fluid density ρ_f (kg/m^3)	1000
Fluid dynamic viscosity μ_f ($Pa \cdot s$)	0.001

5. Results

The parameters varied in the simulations were the fluid inlet velocity and the particle rate. At first, we performed two settling tests in order to obtain the settling velocity of a single sphere and of a particle pack, both in a vertical tube of internal diameter 25.4 mm-ID and filled with the same fluid as described in Tab. 1. We found that the settling velocities were, respectively, $U_t = 0.12$ m/s and $U_t = 0.075$ m/s. Based on these results, we investigated three fluid velocities at the inlet: a smaller, an equal and a higher velocity than the settling velocity of the pack of spheres. Those are presented in Tab. 2.

To define the rate of particles to be inserted in the domain, at first it was set a large particle rate for each one of the velocities configurations. We found that there is a maximum particle rate associated with each distinct fluid velocity, which is a monotonic function of them. We called the maximum particle rate as the saturation state. Other three simulations were carried out, with a particle rate equal to half of the saturation rate for each velocity. The particle rates investigated in this work are also presented in Tab. 2.

Two regions of interest in the domain were chosen to evaluate the particle dynamics: one in the horizontal portion and one in the vertical portion of the pipe. Both have a length of 1D and they corresponds to the red sections of Fig. 2. The horizontal section begins at a distance of 1.5D from the pipe inlet. The vertical section begins at a distance of 4D from the outlet. The velocity magnitude of the particles passing through this two regions was acquired and the mean value was computed over the entire time-span for the six simulations. The results are presented in Tab. 2

The mean velocity magnitude of the particles in the horizontal and vertical sections were close to the fluid velocity for the saturated states, i.e., cases I, III and V, with the average in the vertical section being marginally smaller than the horizontal section. Reducing the particle rate by half, the mean particle velocity magnitude in both sections also reduce, approximately, by a fraction of 40% and 20% in the horizontal and vertical section, respectively. In the half-saturated state, cases II, IV and VI, we observe that the vertical mean velocity is higher than the horizontal one, which is an opposite

Table 2: Parameters investigated.

Case	Fluid velocity (m/s)	Particle rate (particles/s)	Flow state	Particle average velocity magnitude	
				Horizontal sec.[a]	Vertical sec.[b]
I	0.06	109.0392	Sat.[c]	0.054607	0.052464
II		50.0698	Half-sat.[d]	0.028967	0.041454
III	0.08	143.8901	Sat.	0.075467	0.071670
IV		65.5501	Half-sat.	0.043952	0.054576
V	0.10	175.6922	Sat.	0.096593	0.091644
VI		78.3366	Half-sat.	0.06156	0.074424

[a] Horizontal section; [b] Vertical section; [c] Saturation; [d] Half-saturation;

behavior of the saturated state. With a smaller particle rate, more particles tend to settle on the bottom of the horizontal section, reducing their average velocity in that section. The fluid is then accelerated on the upward part of the horizontal tube, increasing the velocity of particles that reach the vertical section.

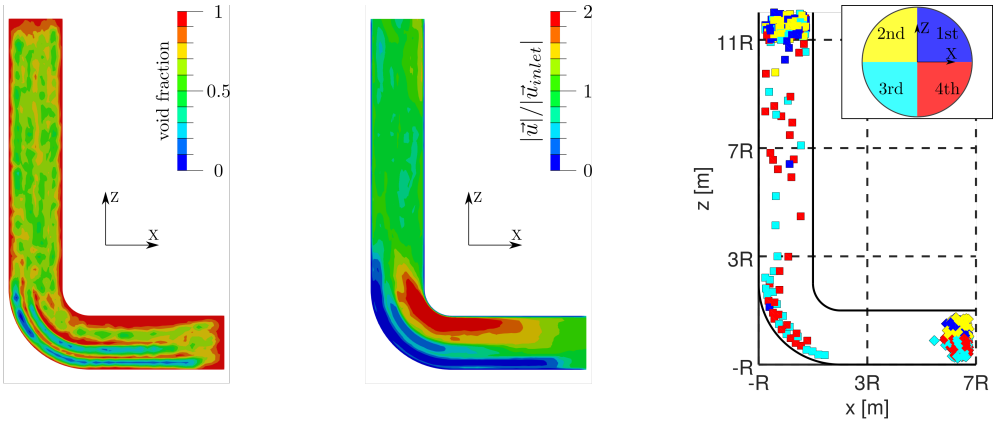

(a) Mean void fraction field.

(b) Mean velocity field normalized by bulk velocity.

(c) Particles initial and final position.

Figure 3: Overview of the simluation - Case IV.

The reduction in the particle rate also changes the flow pattern. While in the saturated cases the particles flow in a more uniform way throughout the entire pipe, the reduction in the particle rate enhances the permanence of particles in the horizontal section and the accumulation of particles in the convex part of the elbow. Figure 3 shows an overview of the simulation of the case IV, where it is depicted the time-averaged of the void fraction field as well as the mean velocity field normalized by the fluid bulk velocity. The average of both fields were computed after the particles began to exit the domain and the system reached the steady state.

In Fig. 3a it can be observed that there is a region of low mean void fraction in the horizontal portion of the pipe and that it extends to the bend region. This low void fraction region resembles to two layers of particles stacked, suggesting that particles tend to take more time to pass through this region or even get confined. Figure 3b show the influence of the particles disposition in the fluid velocity. We can notice the contrast in the mean velocity field in the same region that the low void fraction values are located, i.e., the bottom horizontal portion of the pipe extending to the curve. Here we have two distinct layers, one of high mean velocity and other with a low mean velocity. They can be explained by the particles confined in the low portion of the horizontal section, which accelerate the fluid flow on the upper portion.

The particles initial and final positions were also analyzed and are plotted in Fig. 3c. The initial position is marked by a diamond symbol and the final position by a square one. The markers were colored based on the pipe quadrant of insertion according to the legend of the figure. Only particles that were inserted in a time $t \leq 4\ s$ are shown on the plot.

That corresponds to half of the entire simulation time-span. It can be seen from Fig. 3c that there is a high concentration of particles in the elbow region, which is in accordance with the previous observations of the void fraction and velocity mean fields. It can also be noticed that the particles in the elbow region are supplied mainly by the first and second quadrant. It is worth noticing the presence of some particles also in the vertical section. These particles remain fluctuating for, at least, $4\ s$.

6. Conclusion

In this work, we investigated numerically the dynamics of a solid-liquid flow through a 90° elbow bend with a radius of curvature equals the diameter of the pipe. The pipe had an internal diameter of 25.4mm-ID, with a horizontal section of length 2.5D and the vertical section of 5D. We make use of the open-source software CFDEM to perform the simulations using a resolved method. The method was first validated with experimental results, in particular by means of the drag coefficient for a range of Reynolds number varying from 1 to 1000. The simulation results showed good agreement with the experimental ones, specially for an initial mesh refinement of 6 cells per particle diameter and with a dynamic mesh refinement of level 2.

The same mesh configuration was used in the later simulations tough the refinement in the flow direction was coarser. The main simulations were analyzed by considering three fluid bulk velocities and two particle rate for each velocity. We observed that the simulations with the saturation particle rate have a mean velocity magnitude of the particles almost equal the bulk velocity, both in the horizontal and vertical sections, with the horizontal one being slightly larger. When reducing the particle rate by half, the particles velocities also decreased, but now, the mean velocity of the vertical section was the larger one. In the half-saturated states, particles tend to stay for a long period of time in the elbow region of the pipe. This behavior was corroborated by the analysis of the average void fraction and fluid velocity field. This study shed some light in the comprehension of solid-liquid flow in such scenarios.

7. Acknowledgements

The authors would like to thank the National Council for Scientific and Technological Development - CNPq (Grant No. 144544/2019-9) and the São Paulo Research Foundation - FAPESP (Grant. Nos. 2018/14981-7 and 2019/20888-2) for the financial support provided.

8. References

Bourgoyne Jr, A. *et al.*, 1989. "Experimental study of erosion in diverter systems due to sand production". In *SPE/IADC drilling conference*. Society of Petroleum Engineers, pp. SPE–18716–MS.

Brown, P.P. and Lawler, D.F., 2003. "Sphere drag and settling velocity revisited". *Journal of environmental engineering*, Vol. 129, No. 3, pp. 222–231.

Chen, X., McLaury, B.S. and Shirazi, S.A., 2004. "Application and experimental validation of a computational fluid dynamics (cfd)-based erosion prediction model in elbows and plugged tees". *Computers & Fluids*, Vol. 33, No. 10, pp. 1251–1272.

Cundall, P.A. and Strack, O.D., 1979. "A discrete numerical model for granular assemblies". *geotechnique*, Vol. 29, No. 1, pp. 47–65.

Cúñez, F.D. and Franklin, E., 2019. "Plug regime in water fluidized beds in very narrow tubes". *Powder technology*, Vol. 345, pp. 234–246.

Cúñez, F.D. and Franklin, E.M., 2020. "Crystallization and jamming in narrow fluidized beds". *Physics of Fluids*, Vol. 32, No. 8, p. 083303.

Di Renzo, A. and Di Maio, F.P., 2004. "Comparison of contact-force models for the simulation of collisions in dem-based granular flow codes". *Chemical engineering science*, Vol. 59, No. 3, pp. 525–541.

Duran, J., 2012. *Sands, powders, and grains: an introduction to the physics of granular materials*. Springer Science & Business Media.

Hager, A., Kloss, C., Pirker, S. and Goniva, C., 2012. "Parallel open source cfd-dem for resolved particle-fluid interaction". In *Proceedings of 9th International Conference on Computational Fluid Dynamics in Minerals and Process Industries*. pp. 1–6.

Kloss, C., Goniva, C., Hager, A., Amberger, S. and Pirker, S., 2012. "Models, algorithms and validation for opensource dem and cfd–dem". *Progress in Computational Fluid Dynamics, an International Journal*, Vol. 12, No. 2-3, pp. 140–152.

Li, Y., Zhang, H., Lin, Z., He, Z., Xiang, J. and Su, X., 2019. "Relationship between wear formation and large-particle motion in a pipe bend". *Royal Society open science*, Vol. 6, No. 1, p. 181254.

Mondal, S., Wu, C.H. and Sharma, M.M., 2016. "Coupled cfd-dem simulation of hydrodynamic bridging at constrictions". *International Journal of Multiphase Flow*, Vol. 84, pp. 245–263.

Parsi, M., Najmi, K., Najafifard, F., Hassani, S., McLaury, B.S. and Shirazi, S.A., 2014. "A comprehensive review of solid particle erosion modeling for oil and gas wells and pipelines applications". *Journal of Natural Gas Science and Engineering*, Vol. 21, pp. 850–873.

Peng, W. and Cao, X., 2016. "Numerical prediction of erosion distributions and solid particle trajectories in elbows for gas–solid flow". *Journal of Natural Gas Science and Engineering*, Vol. 30, pp. 455–470.

Peskin, C.S., 1972. "Flow patterns around heart valves: a numerical method". *Journal of computational physics*, Vol. 10, No. 2, pp. 252–271.

Shirazi, S., Shadley, J., McLaury, B. and Rybicki, E., 1995. "A procedure to predict solid particle erosion in elbows and tees". *Journal of Pressure Vessel Technology*, pp. 45–52.

Shirgaonkar, A.A., MacIver, M.A. and Patankar, N.A., 2009. "A new mathematical formulation and fast algorithm for fully resolved simulation of self-propulsion". *Journal of Computational Physics*, Vol. 228, No. 7, pp. 2366–2390.

Uzi, A. and Levy, A., 2018. "Flow characteristics of coarse particles in horizontal hydraulic conveying". *Powder Technology*, Vol. 326, pp. 302–321.

Vaezi, M., Verma, S. and Kumar, A., 2018. "Application of high-frequency impedancemetry approach in measuring the deposition velocities of biomass and sand slurry flows in pipelines". *Chemical Engineering Research and Design*, Vol. 140, pp. 142–154.

Zhang, H., Tan, Y., Yang, D., Trias, F.X., Jiang, S., Sheng, Y. and Oliva, A., 2012. "Numerical investigation of the location of maximum erosive wear damage in elbow: Effect of slurry velocity, bend orientation and angle of elbow". *Powder Technology*, Vol. 217, pp. 467–476.

Zhou, M., Wang, S., Kuang, S., Luo, K., Fan, J. and Yu, A., 2019. "Cfd-dem modelling of hydraulic conveying of solid particles in a vertical pipe". *Powder Technology*, Vol. 354, pp. 893–905.

Zhou, Z., Kuang, S., Chu, K. and Yu, A., 2010. "Discrete particle simulation of particle–fluid flow: model formulations and their applicability". *Journal of Fluid Mechanics*, Vol. 661, pp. 482–510.

Zhu, H., Zhou, Z., Yang, R. and Yu, A., 2007. "Discrete particle simulation of particulate systems: theoretical developments". *Chemical Engineering Science*, Vol. 62, No. 13, pp. 3378–3396.

Zhu, H., Zhou, Z., Yang, R. and Yu, A., 2008. "Discrete particle simulation of particulate systems: a review of major applications and findings". *Chemical Engineering Science*, Vol. 63, No. 23, pp. 5728–5770.

9. RESPONSIBILITY NOTICE

The following text, properly adapted to the number of authors, must be included in the last section of the paper: The author(s) is (are) solely responsible for the printed material included in this paper.